Environmental Gamma Dose Rate Measurements using CZT Detectors

Sebastian Kreutzer, Loïc Martin, Didier Miallier, Norbert Mercier

Environmental Gamma Dose Rate Measurements using CZT Detectors

Sebastian Kreutzer[1, *], Loïc Martin[2], Didier Miallier[3], and Norbert Mercier[4]

[1]Institute of Geography, Heidelberg University, Im Neuenheimer Feld 348, 69120 Heidelberg, Germany
[2]Innsbruck Quaternary Research Group, University of Innsbruck, Innrain 52, 6020 Innsbruck, Austria
[3]Laboratoire de Physique de Clermont-Ferrand, Université Clermont Auvergne, Campus des Cézeaux, 24, avenue des Landais BP 80026, 63171 Aubière cedex, France
[4]Archéosciences Bordeaux, CNRS-Université Bordeaux Montaigne, Maison de l'Archéologie, Esplanade des Antilles, 33607 Pessac cedex, France

Correspondence: Sebastian Kreutzer (sebastian.kreutzer@uni-heidelberg.de)

Abstract. The accurate and precise determination of the environmental dose rate is pivotal in every trapped-charge dating study. The environmental gamma-dose rate component can be determined from radionuclide concentrations using conversion factors or directly measured in situ with passive or active detectors. In-field measurements with an active detector are usually inexpensive and straightforward to achieve with adequate equipment and calibration. However, despite the rather widespread use of portable NaI or $LaBr_3$ scintillator detectors, there is a lack of research on the performance and practicality of portable alternative detectors in dating studies, particularly in light of newer developments in the semi-conductor industry. Here, we present our experience with two small portable semi-conductor detectors housing Cadmium Zinc Telluride (CZT) crystals. Given their small volume and low power consumption, we argue they present attractive alternatives for gamma-dose rate measurements in dating studies. Despite high relative detection efficiency, their small volume may pose different challenges, resulting in impractical measurements in routine studies and, therefore need investigation. In our study, we simulated the particle interaction of the CZT crystal with GEANT4 in different sediment matrices to quantify the energy threshold in the spectrum above which the count/energy-count rate correlates with the environmental gamma dose-rate irrespective of the origin of the gamma-photons. We compared these findings with dose-rate calibration curves constructed from reference sites in France and found a good agreement in settling on a threshold at $197\,\mathrm{keV}$. We additionally report negligible equipment background and required minimal measurement time of only $20\,\mathrm{min}$ in typical environments. Cross-checking our calibration on a homogenous loess deposit near Heidelberg confirmed the setting and assumed performance through a nearly identical gamma-dose rate of $1105 \pm 105\,\mu\mathrm{Gy\,a^{-1}}$ (CZT) to $1124 \pm 25\,\mu\mathrm{Gy\,a^{-1}}$ (laboratory) The outcome of our study gives credit to our threshold definition. It validates the similarity of the two investigated probes, which may make it straightforward for other laboratories to implement the technique effortlessly. Finally, the implementation of CZT detectors has the potential to streamline fieldwork and enhance accuracy and precision of trapped-charge dating-based-chronologies.

1 Introduction

The ascertainment of the effective environmental dose rate is indeed crucial for accurate and precise ages in luminescence and electro-resonance (short: trapped-charge) dating studies. The dose rate plays a vital role in the age equation as it is a significant factor in determining the amount of radiation absorbed over time.

Field procedures typically involve sampling sufficient bulk material around the sampling site. T he material is then analysed to quantify the natural radionuclide concentrations (such as U, Th, and K concentrations) as major contributors to the environmental radiation. If collecting sufficient material is not feasible around the sampling site, e.g., in archaeological excavations, the required material can be carefully separated from the to-be-dated material combined with in situ measurements.

Strategies to ensure a good environmental dose rate estimation ideally interoperate both, laboratory and field, measurements. Standard analytical methods in the laboratory involve α-/$\beta-$counting, γ-ray spectrometry (e.g., Aitken, 1985; Zöller and Pernicka, 1989; Hutton and Prescott, 1992; Preusser and Kasper, 2001; Godfrey-Smith et al., 2005; Mauz et al., 2021; Kolb et al., 2022) and element analytical methods such as inductively coupled plasma mass spectrometry (ICP-MS) (e.g., Preusser and Kasper, 2001) or a combination of those methods. Activity or element concentrations are then converted for each type of radiation (α-, β, γ-radiation) using dose-rate conversion factors (latest update: Cresswell et al., 2018).

Dose-rate (γ- and, more challenging, β-) components can be measured in the field at the sampling position using passive dosimeters (e.g., Hutton and Prescott, 1992; Kalchgruber et al., 2003; Kalchgruber and Wagner, 2006; Richter et al., 2010; Kreutzer et al., 2018) stored over a couple of weeks to months or with active detectors (usually γ-ray probes) (e.g., Mercier and Falguères, 2007; Guérin and Mercier, 2011; Arnold et al., 2012; Bu et al., 2021; Martin et al., 2024) enabling nearly instant dose rate estimates.

Regardless of the preferred method and type of detector, active or passive, in-field measurements appeal when sampling suggests a heterogeneous distribution of radionuclides or complex geometries (e.g., the close succession of very different sediment layers, gravels/rocks in the profile). The field dose-rates can later be compared to laboratory results based on the radionuclide concentrations. Ideally, the obtained numbers agree within uncertainties, or the discrepancy gives further insight into the site's matrix composition. Active detectors can be paired with a portable luminescence reader (e.g., Sanderson and Murphy, 2010) to profiles' stratigraphy and determine relative chronologies. A rule of thumb would approximate the γ-dose component as about 28% to 36% of the total dose rate (numbers derived from the ChronoLoess database by Bosq et al., 2023; alternatively, see estimates in Aitken, 1985). These numbers underpin the importance of the γ-dose rate contribution and its significance in estimating accurate trapped-charge ages.

On the flip site, the usually short measurement durations, compared to the expected age of the sediment, has the disadvantage that long-term changes in the water content are not reflected. Furthermore, depending on the size of the detector probe a rather large hole with a depth of at least ca $30\,\mathrm{cm}$ is required for the measurement. Such a hole is sometimes difficult to dig, not always possible (samples from a drilled core) or not favoured given the setting (e.g., archaeological excavation). Here focussing on active detectors, additional everyday challenges involve equipment calibration and handling usually proprietary hardware such as cables or multi-channel analysers that are costly to repair or even unavailable after they have been phased out by the

manufacturer. Last, the equipment can be bulky, especially for large detectors (up to $3 \times 3\,\mathrm{in}$ for a portable NaI probe) and, given first-hand experience, the equipment is prone to preferred inspection during air travel.

In summary, while in-field measurements with active detectors do present certain challenges, their benefits are still considerable. They provide valuable, real-time data at a relatively low cost, significantly improving the accuracy of dating studies. As a result, their routine use seems advisable.

In the following, we will test two commercially available portable Cadmium Zinc Telluride (CZT) detectors for in situ γ-ray measurements. The detectors are small and highly portable, and we assume that they can pose an alternative to systems using larger NaI or $LaBr_3$ probes in trapped-charge dating applications. Next, we will begin outlining the technical specifications and advantages of the CZT systems. We will then detail the required calibration methods and explore the performance and dose-response characteristics of the detectors through simulations and measurements in different natural sites with well-known radionuclide concentrations. Finally, we will test the calibrated systems in a loess deposit near Heidelberg and discuss the results.

In this contribution, we focus exclusively on the "threshold" technique for measuring environmental γ-dose rates ($\dot{D}\gamma$ in $\mu\mathrm{Gy}, \mathrm{a}^{-1}$). Unlike the "window" method, which compares the area under a specific γ-peak in a sample with unknown composition to the area of a γ-peak in a sample with known radionuclide composition, the threshold technique integrates the entire spectrum above a set threshold. The threshold approach provides a direct measure of $\dot{D}\gamma$ in $\mu\mathrm{Gy}, \mathrm{a}^{-1}$ rather than a radionuclide concentration.

2 Material and methods

2.1 Brief background γ-detectors

Measuring γ-rays translates to observing the interaction of (γ-) photons with matter by quantifying the production of secondary charged particles. Suitable are scintillation detectors such as NaI(Tl) or $LaBr_3$ collecting light caused by the interaction of the γ-photons with the detector material or semiconductor-based detectors (e.g., high-purity Ge) that, combined with a suitable electronics, record the amount of produced secondary-hole pairs (e.g., Gilmore, 2008).

To measure γ-rays outside a laboratory, for instance, in trapped-charge dating studies, portable detectors that can be operated at room temperature are preferred. This usually favours scintillation detectors using NaI(Tl) or $LaBr_3$ with typical probes ranging from $1.5 \times 1.5\,\mathrm{in}$ to $3 \times 3\,\mathrm{in}$ over HPGe semiconductor-based detectors that require operation at liquid nitrogen temperature due to small band-gap of the crystal. Cadmium Zinc Telluride (CZT and CdZnTe) were proposed as promising alternatives with better γ-ray absorption performance and operational at room temperature. However, the production process is more challenging (e.g., Gilmore, 2008) and such detectors were not an option considered in the context of trapped-charge geochronology; yet.

Since the 1990s, the development of CZT semiconductor detectors progressed considerably in their applicability as γ-ray (for reviews, see Scheiber and Chambron, 1992; Verger et al., 1997; Limousin, 2003; Alam et al., 2021). They offer a small volume and operate at ambient temperature by collecting charges created by the interaction of ionising radiation with a high

relative efficiency for photoelectric interaction (atomic numbers Cd: 48, Te: 52; density crystal ca $5.8\,\mathrm{g\,cm^{-3}}$) (Limousin, 2003; Alam et al., 2021). Although this is less important in our case, they provide an energy resolution comparable to or better than $LaBr_3$ and considerably higher than NaI(Tl) (Alexiev et al., 2008) probes. Although given the small volume available, the absolute efficiency is lower than that of larger detectors. This feature, combined with a low energy consumption, renders this detector type particularly appealing for our application.

2.2 Equipment

For our experiments, we used two systems from Kromek (https://www.kromek.com/; last access: 2024-08-17) with CZT detectors. (1) RayMon10® (henceforth: RayMon GR1) and (2) GR1+® (henceforth: GR1)[1] (Fig. 1). Both systems include a similar $10 \times 10 \times 10\,\mathrm{mm^3}$ GR1 CZT detector connected to a 4096 energy/channels analyser. The detection ranges from $30\,\mathrm{keV}$ to $3\,\mathrm{MeV}$ with an energy resolution of around 2.5% FWHM at $662\,\mathrm{keV}$. The RayMon GR1 was delivered with a handheld touch-screen device running Microsoft Windows 10® and comes housed. The probe communicates with the handheld device via a Universal Serial Bus (USB) Type A connector. The battery lasts around eight to ten hours, depending on the display brightness setting. Although much smaller in housing size ($25\,\mathrm{mm} \times 25\,\mathrm{mm} \times 63\,\mathrm{mm}$, $60\,\mathrm{g}$), the GR1 contains a similar CZT detector. It has a Mini-A USB port that can be attached to any standard computer given a suitable cable and operated using the software K-Spect® that can be downloaded free of charge from the manufacturer. The GR1 consumes only $250\,\mathrm{mW}$ and is hence operational as long as the battery of the connected computer lasts. For more information, we refer to the manufacturer's website.

Because the Mini-USB port of the GR1® seemed fragile, and we were not sure about the sealing of the housing against moisture, we designed a 3D-printed, rubber-sealed strain-relief mount (Fig. 1) and attached it to the detector housing. The strain relief enables safe retrieval of the detector, and the plastic bag wrapping keeps dirt and moisture away during field operations. We share the print-ready `*.stl` file under CC BY 4.0 licence conditions along with this article.

2.3 Calibration methods

We aim to use the detectors in routine dating applications to determine $\dot{D}_\gamma$ in $\mu\mathrm{Gy\,a^{-1}}$. This requires three separate experiments in given order to set up each device device: (1) Channel/energy calibration, (2) energy threshold definition, and (3) a calibration curve modelling counts against the environmental dose rate.

2.3.1 Channel/energy calibration

The channel/energy calibration (Sec. 3.1) assigns energy values in keV to the, in our case, 4096 channels. The calibration makes it easier to interpret the γ-ray spectrum, enables a comparison of spectra, and accounts for shifts in the spectrum that may occur due to, for instance, changed environmental conditions.

[1]The plus indicates a slightly higher energy resolution compared to the "non-plus" GR1 version.

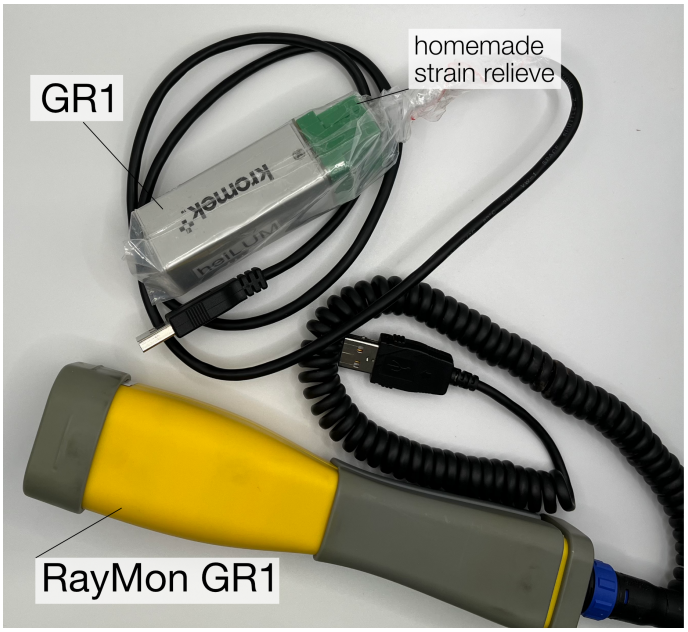

Figure 1. Kromek detectors used for our measurements (shown is the probe without the handheld tablet PC for the RayMon10®). Both probes house a similar CZT detector. We wrapped the GR1® in a standard plastic bag and attached a home made strain-relieve to the GR1® to enable easier operation and retraction of the detector in the field.

Both detectors used here were delivered with a test and inspection sheet documenting measurements against ^{241}Am (γ-line at $59.5\,\mathrm{keV}$) and ^{137}Cs (γ-line at $662\,\mathrm{keV}$). The results are nearly identical for both detectors with an offset of ca $2\,\mathrm{channels/keV}$ between the GR1 and the RayMon GR1.

For the channel/energy calibrations, where only the peak position matters, we used two γ-standards available in Heidelberg closely arranged around the detector for two measurements over $3600\,\mathrm{s}$. One radiator is a home-made uranium standard (U concentration: 1.02%) and other an Amersham EB 165 mixed radionuclide standard with ^{241}Am and ^{137}Cs. The Amersham standard also contains other shorter-lived radionuclides; however, given the age of the standard (>30 years), we do not expect to observe significant counts above background within the chosen measurement time.

2.3.2 Energy threshold determination

The energy-threshold definition (Sec. 3.5) determines the threshold in the spectrum above which $\dot{D}_\gamma$ is seemingly independent of the origin of the absorbed γ-photons (see Løvborg and Kirkegaard, 1974, for details). In other words, the integrated spectrum above the threshold is used to derive $\dot{D}_\gamma$. Guérin and Mercier (2011) distinguished two different thresholds techniques for *integrating* the spectrum. The "count" and the "energy" threshold (integration technique). The *count* threshold adds all counts above a certain threshold (η) whereas the *energy* threshold integrates the deposited energy above η. Assuming that S_i is the signal registered either as absolute counts ($\mathrm{cts\,ch^{-1}}$) or count rate ($\mathrm{cts\,ch^{-1}\,s^{-1}}$) in the i^{th} channel of the spectrum, E_i in keV

the energy associated with a certain channel. For the counting threshold technique, the relationship between the environmental γ-dose rate and integrated value above the threshold for an energy/channel calibrated spectrum becomes

$$\dot{D}_\gamma \sim \Sigma_{i:=\eta}^{N} S_i \tag{1}$$

and it reads

$$\dot{D}_\gamma \sim \Sigma_{i:=\eta}^{N} S_i \times E_i \tag{2}$$

for the energy threshold integration technique. Guérin and Mercier (2011) found η slightly lower for the latter technique, resulting in a larger proportion of the spectrum usable, which lowers the statistical uncertainty. Although related, the two threshold integration techniques must be distinguished from quantifying η, i.e. finding the energy above which $\dot{D}_\gamma$ is a function of the integrated counts (Løvborg and Kirkegaard, 1974); regardless of the integration technique.

To determine η, one can perform modelling (e.g., Guérin and Mercier, 2011) or measure the γ-ray spectra of "pure" emitters of known U, Th, K concentrations (Mercier and Falguères, 2007; Rhodes and Schwenninger, 2007; Duval and Arnold, 2013).

For our contribution, we modelled the threshold (henceforth: η_{sim} in keV) using *GEANT4* (Agostinelli et al., 2003) using three different sediment matrices: (1) A SiO_2 matrix consisting #TODO Loïc, (2) an iron rich clay matrix, and (3) a calcite rich clay matrix #TODO Loïc.

#TODO: @Loïc: Please provide a few lines with reference about the simulations

We compare these findings with measurements at three natural calibration sites available in the vicinity of Clermont-Ferrand (France) (Miallier et al., 2009) and the home-made brick block in the cellar of the Archéosciences Bordeaux laboratory (Richter et al., 2010) to derive η_{exp}. The investigated sites (Fig. 2) have a well-known radionuclide composition from which $\dot{D}_\gamma$ can be calculated to construct γ-dose rate calibration curves using the two threshold integration technique to re-evaluate η as the value where the mean square of residuals from the model reaches the lowest value. The underlying assumption of this approach is that if the threshold was set correctly, the regression line should exhibit the best fit as a non-ideal threshold should increase the residuals due to a poor fit. Insufficient model adaptation is caused by poor counting statistics (threshold too large) or in situations where the prerequisite of the technique that $\dot{D}_\gamma$ is independent of the origin of the γ-photons is not fulfilled (threshold too low).

2.3.3 Dose-rate calibration curves

The dose-rate calibration curve (Sec. 3.6) correlates the integrated (count and energy integration technique) signal with $\dot{D}_\gamma$ from the reference sites (Table 1), i.e. the response of the detector to natural γ-radiation. If established, it allows us to derive an accurate estimate of $\dot{D}_\gamma$ from a natural site with unknown radionuclide composition. As pointed out by Guérin and Mercier (2011), the water content will not affect the counting rate significantly, and the established value should be applicable to sites usually probed in trapped-charge dating applications.

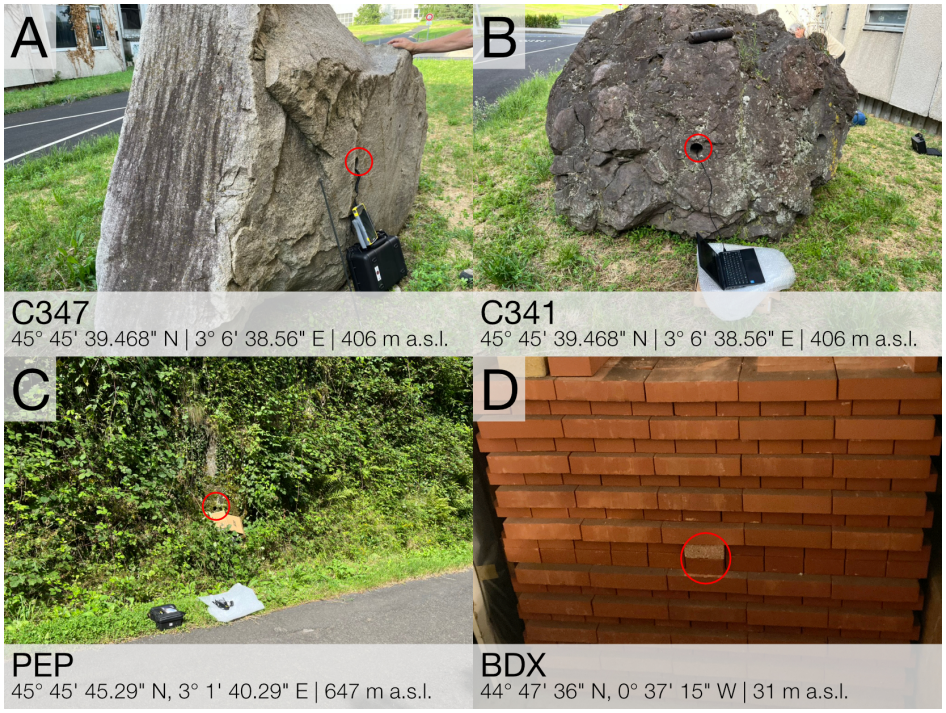

Figure 2. Photos of the calibration sites with known radionuclide composition. Further details can be found in Miallier et al. (2009) and Richter et al. (2010). The red circles mark the measurement positions (holes) for the probe. The site BDX is located in the basement of the Archéosciences Bordeaux laboratory at the Université Bordeaux Montaigne in Pessac an not accessible to the public.

Table 1. Known γ-dose rates from reference sites. The dataset listed here ships with the 'gamma' R package. In the original dataset BDX is termed BRIQUE, which is the brick block in the Archéosciences Bordeaux laboratory, for clarity, we relabeled it to BDX for our analysis. We list the results calculated with the conversion factors by Cresswell et al. (2018).

SITE	**NATURE**	**U**	σ_U	**Th**	σ_{Th}	**K**	σ_K	$\dot{D}_\gamma$	$\sigma_{\dot{D}_\gamma}$
BDX	ceramic	4.1	0.1	13.7	0.4	3.5	0.1	1997.1	37.7
C341	trachybasalt	1.8	0.0	6.4	0.4	1.4	0.0	855.2	21.8
C347	granite	2.8	0.1	4.7	0.1	3.5	0.1	1425.5	27.4
PEP	granite	6.0	0.2	19.0	2.0	3.8	0.2	2554.3	112.7

Note:

U, Th concentrations in $\mu g\, g^{-1}$, K in % | dose rates in $\mu Gy\, a^{-1}$.

The $\dot{D}_\gamma$ values in Table 1 differ from the values reported in Miallier et al. (2009) after we recalculated them using the conversion factors compiled by Cresswell et al. (2018). Values recalculated for other conversion factors can be found in the dataset `clermont_2024` contained in the R `'gamma'` package (> v1.0.5).

Please note that for establishing the calibration curves we assumed "infinitive matrix" conditions that enabled us to convert the radio-nuclide concentrations into dose rates (e.g., Guérin et al., 2012, for a critical review of this concept).

2.4 Radionuclide determination cross-check

To validate our calibration and post-processing procedure, we recorded natural γ-spectra at the Weiße Hohl. The site is a gully of anthropogenic origin that cut into the famous last-glacial aeolian deposits near Nussloch (Germany) (e.g., Antoine et al., 2001). Today, the gully is part of a hiking trail in the area and hence easily accessible. The Nussloch loess deposits are well-investigated through numerous studies, and the expected $\dot{D}_\gamma$ at Weiße Hohl was about $1000\,\mu\mathrm{Gy\,a^{-1}}$ (Rieser, 1991). What made the measurements at this particular further interesting was that loess is a typical environment subject to past climate and chronology studies using trapped-charge dating methods.

We recorded two spectra over $20\,\mathrm{min}$ with both detectors in a $32\,\mathrm{cm}$ deep hole and sampled about $120\,\mathrm{g}$ of material for subsequent radionuclide and gravimetric water content quantification. For measuring the natural radionuclide concentrations, we employed a µDose (Tudyka et al., 2018; Kolb et al., 2022) and a µDose+ (Tudyka et al., 2024) system on the same $3\,\mathrm{g}$ subsample. The sample was measured more than two days each.

To compare the $\dot{D}_\gamma$ calculated from the radionuclide concentrations using the conversion factors by Cresswell et al. (2018) and we corrected the $\dot{D}_\gamma$ measured with GR1 and RayMon GR1 for the field water content (Aitken, 1985).

2.5 Data and data processing

We used *GEANT4* (Agostinelli et al., 2003) for the threshold modelling and processed our data with R (R Core Team, 2024) and the packages `'gamma'` (Lebrun et al., 2020; Frerebeau et al., 2024) and `'ggplot2'` (Wickham, 2016). The two investigated Kromek measurement systems provide export functionality for various data formats. We opted for the ASCII format `.spe` and added support in the function `gamma::read()` to the package `'gamma'` (> v1.0.5) for this study (Frerebeau et al., 2024). Except additions detailed below, our workflow follows the suggestions by Lebrun et al. (2020) and the tutorials that come with the `'gamma'` (> v1.0.5) R package. To ensure that the figures have colour-blind-friendly colours, we used the R package `'khroma'` (Frerebeau, 2024). A shortened version of the R code used for all the calculations, data, and calibration output are available on Zenodo (Kreutzer et al., 2024) under CC BY 4.0 licence conditions in accordance with common data-sharing guidelines. Please note that in order to run the R code used for this contribution you will need to run the developer version of `'gamma'` (https://github.com/crp2a/gamma; last access: 2024-09-10) since we added a couple of workflow fixes to the package.

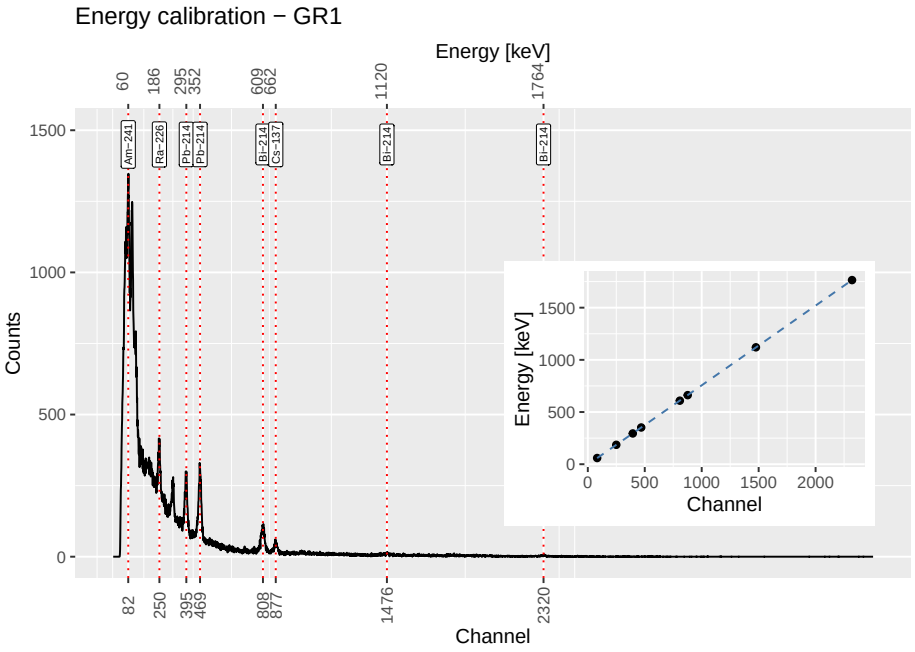

Figure 3. Energy calibration results for detector GR1. The main plot shows the raw spectrum with known γ-lines marked with dashed lines. The inset displays the calibration curve applied to all subsequently shown spectra. Peak positions were found to be similar for GR1 and RayMon GR1.

3 Results

3.1 Energy calibration

Figure 3 shows the spectrum plot of GR1 measured over $3600\,\mathrm{s}$. We placed our γ-standards with known composition in front of the detector. The dashed lines marked the γ-lines used for the channel/energy calibration (peaks at higher energies are better identifiable on a, here not chosen, log-scale). The inset draws the energy/channel-calibration curve applied subsequently to all analysed spectra. We did not apply low-level discrimination and recorded raw count values for the measurements, i.e. the count rate was calculated in the post-processing. We have chosen the measurement time to achieve a good counting statistic.

Given the nuclide composition, we expected to see typical γ-lines present in ^{238}U on top of ^{241}Am and ^{137}Cs. The manufacturer also used the latter two nuclides before delivery to test the CZT detectors' performance and hence they provide a good reference for a cross-check. We manually identified eight γ-lines in our spectrum and assigned the results to the imported spectra with the `gamma::energy_calibrate()` function. To ease the peak identification, we started with the ^{241}Am and ^{137}Cs γ-lines for which we have channel-to-energy references determined by the manufacturer. For instance, the manufacturer specifies to find the $59.5\,\mathrm{keV}$ ^{241}Am peak in channel number 80 ($\pm 10\,\%$) and the $662\,\mathrm{keV}$ ^{137}Cs at 880 ($\pm\,1\,\%$). Our calibration confirmed those values with channel number 82 for ^{241}Am $59.5\,\mathrm{keV}$ and channel number 877 for ^{137}Cs $662\,\mathrm{keV}$.

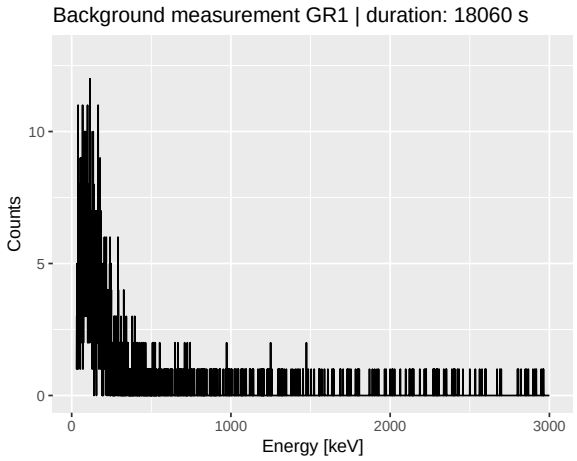

Figure 4. Background measurements with GR1 in the lead castle for more than 5 h. The system background is negligible compared to typical measurements in the field.

The same calibration was performed with the RayMon GR1 detector but with its measurement time reduced to 900 s as a cross-check. We found that the peak positions of RayMon GR1 were virtually identical to GR1 (not shown). Hence, we applied the GR1 channel/energy calibration to all measured spectra, and all spectra shown subsequently are energy/channel-calibrated using the established calibration curve.

3.2 Background measurements

To investigate the detector's counting background, we placed the GR1 for ca 5 h (18060 s) in a lead housing inside a low-level background environment at the PRISNA facility (Plateforme Régionale Interdisciplinaire de Spectroscopie Nucléaire en Aquitaine) near Bordeaux. The facility is a scientific platform used for low-level γ-ray spectroscopy experiments. Figure 4 illustrates that the system background is tiny compared to typical environmental situations. We, therefore, considered the equipment background negligible in our subsequent analyses.

3.3 Energy-calibrated raw spectra

Figure 5 displays all energy calibrated γ-ray spectra measured at the sites at Clermont-Ferrand, Bordeaux and PRISNA. We show count rates instead of absolute count values to account for the different measurement time. The shortest live time was 1200 s (PEP) and the longest 18059 s (PRI). All spectra in Fig. 5(A) and (B) are scaled and colour-coded similarly for better comparison. Site PRI (the background measurement) was only measured with the GR1.

Visible in both spectra is a dominant Compton continuum rather than distinguishable photo peaks. This observation is not surprising given the short measurement time, the low abundance of the radionuclides (e.g., Miallier et al., 2009, for the Clermont-Ferrand sites) and, of course, the relatively low absolute efficiency for the small CZT crystal. It is reassuring that all comparable raw spectra appear very similar in intensity, position and shape, except for the C341 spectra.

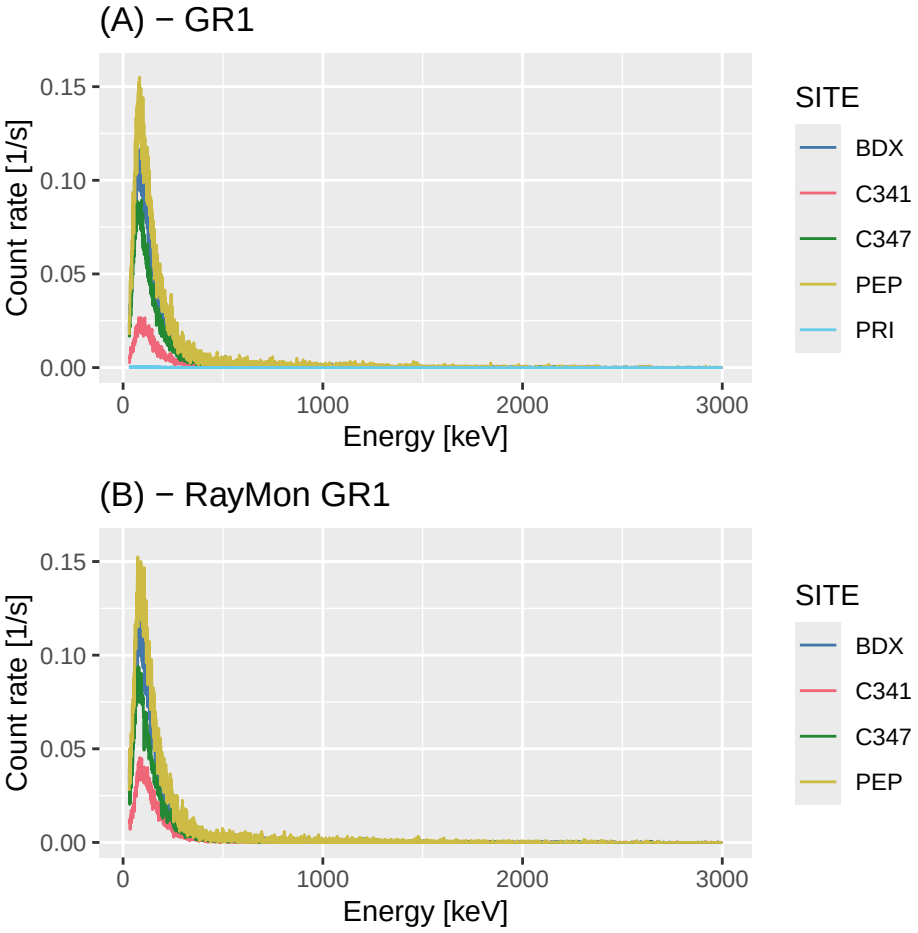

Figure 5. Channel/energy calibrated spectra as recorded in the reference sites as count rate against energy. (A) Spectra measured with detector GR1, (B) spectra measured with detector RayMon GR1. The spectra for both detectors are virtually identical in terms of peak position and count rates. The count rate for spectra C341 is significantly lower in (A) compared to (B). This is due to a software error (see maintext) and therefore this spectrum was discarded. 'PRI' refers to the background spectrum recorded in the lead castle.

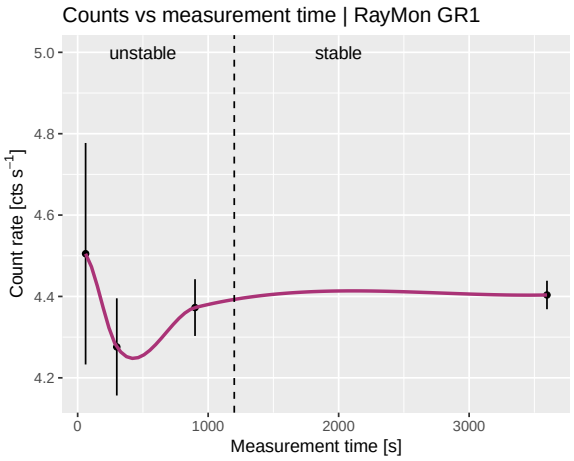

Figure 6. Sum of counts normalised to the measurement time recorded in the brick block at Archéosciences Bordeaux. After 20 min the average count rate does not change anymore within uncertainties. The plot scales depending on the settings of η (the energy threshold) and it was set to the value determined through our experiments.

The spectra recorded in site C341 (a basaltic rock) appear to show only half of the counts measured with detector GR1 compared to the RayMon GR1 detector. This discrepancy is because GR1 was controlled via an external mobile computer that went unexpectedly into sleep mode. After reactivating the computer, the software seemed to have continued counting. However, post-processing revealed that it had stopped registering γ-photons. In other words, the difference between the two readings (GR1 vs RayMon GR1) for C341 is a technical error, and hence, we discarded the spectrum C341 measured with GR1 for subsequent analysis. This error can be avoided easily but we kept it in the manuscript to share our experience.

3.4 Minimum measurement time

When we performed our measurements at the reference sites, we still needed more practical experience with the two detectors. Therefore, we opted for measurement times longer than the typical setting for the $LaBr_3$ probes (ca 10 min). Unfortunately, hour-long measurements for one sampling spot are often impracticable, considerably reducing the practicability of in-field measurements.

To assess the reasonably required measurement time for recordings, defined as a stable count rate within uncertainties in the field, we placed the RayMon GR1 detector in the brick block at Bordeaux (site: BDX) and started measurements for 60 s, 300 s, 900 s, and 3600 s (Fig. 6). Given the similarity of both detectors, we assume that this experiment will also be valid for the GR1. In the post-processing we integrated all spectrum counts for the experiment using the integration settings given below and normalised them to the measurement duration. The count rate is a little bit erratic over the first 500 s before stabilising after 20 min of measurement time. Additional measurement time increases the count rate only slightly. We therefore conclude that 20 min suffice in typical environments to determine a stable signal.

3.5 Threshold definition

In Sec. 2.3, we outlined the concept for defining the optimal energy threshold (η) above which the count rate correlates with the absorbed dose, regardless of the nature of the emitter and the matrix composition. The threshold is, in essence, a function of particle interaction with the (CZT) detector. Løvborg and Kirkegaard (1974) estimated the energy threshold for their setup (3×3 in NaI detector) at $500\,\mathrm{keV}$. Mercier and Falguères (2007) calculated a threshold of $320\,\mathrm{keV}$ for their $1.5 \times 1.5\,\mathrm{in}$ NaI probe, a value later largely confirmed by simulations by Guérin and Mercier (2011) (their threshold value: $296\,\mathrm{keV}$). Also, Duval and Arnold (2013) reported comparable values for NaI and $LaBr_3$ detectors of the same sizes ($LaBr_3$)(Ce): $358\,\mathrm{keV}$, NaI(Tl): $322\,\mathrm{keV}$). As a rule of thumb, the larger the detector (higher absolute efficiency), the further the threshold shifts to higher energies. Since the volume of our CZT detector is small, we would locate the threshold in the low-energy part of the spectrum not higher than the values to be found in the literature.

3.5.1 GEANT4 simulations

Figure 7 exhibits the simulations results for the three different matrices. We show the relative standard deviation between the spectra of the radionuclides of the U- and Th-series and the ^{40}K. We defined the energy threshold η_{sim} for the situation in which the relative standard deviations for all three matrices fall below $10\,\%$ (vertical dashed line in Fig. 7). This gives a nice energy threshold plateau between 192.5 keV and 242.5 keV.

@Loïc: Perhaps you want to add something?

3.5.2 Field measurements

To estimate the threshold for our systems, we calculated the γ-dose rate response curve for different energy windows using `gamma::dose_fit()`. Amongst other values, the function returns the mean square of the residuals (MSWD), which we can use to approximate the quality of fit of our regression model. We defined the moving lower energy limit as E_i ($i := \{30, ..., 1000\}$) and E_{max} was set to $2800\,\mathrm{keV}$ to avoid counts from cosmic-rays. Figure 7B shows the outcome of this calculation for both detectors (blue: GR1, red: RayMon GR1). The results of the two calculations differ significantly, and given the similarity of the detectors, one may have expected a better match. We believe that this deviation is caused by the discarded data point C341 for GR1, which is the lower point in the calibration curve. Therefore, we decided to use only the data for RayMon GR1 to determine the threshold η_{exp}.

For the counting *calculation* technique (not shown in Fig 7B), the minimum in the search window between $30\,\mathrm{keV}$ and $350\,\mathrm{keV}$ was found at 217 keV. For the energy counting *calculation* technique, we located the value at 182 keV. Given the simulation results and considering stochastic uncertainties, we decided to combine $min(\eta_{sim})$ and $min(\eta_{exp})$ and use the arithmetic average of 197 keV as suitable value for η for subsequent analysis.

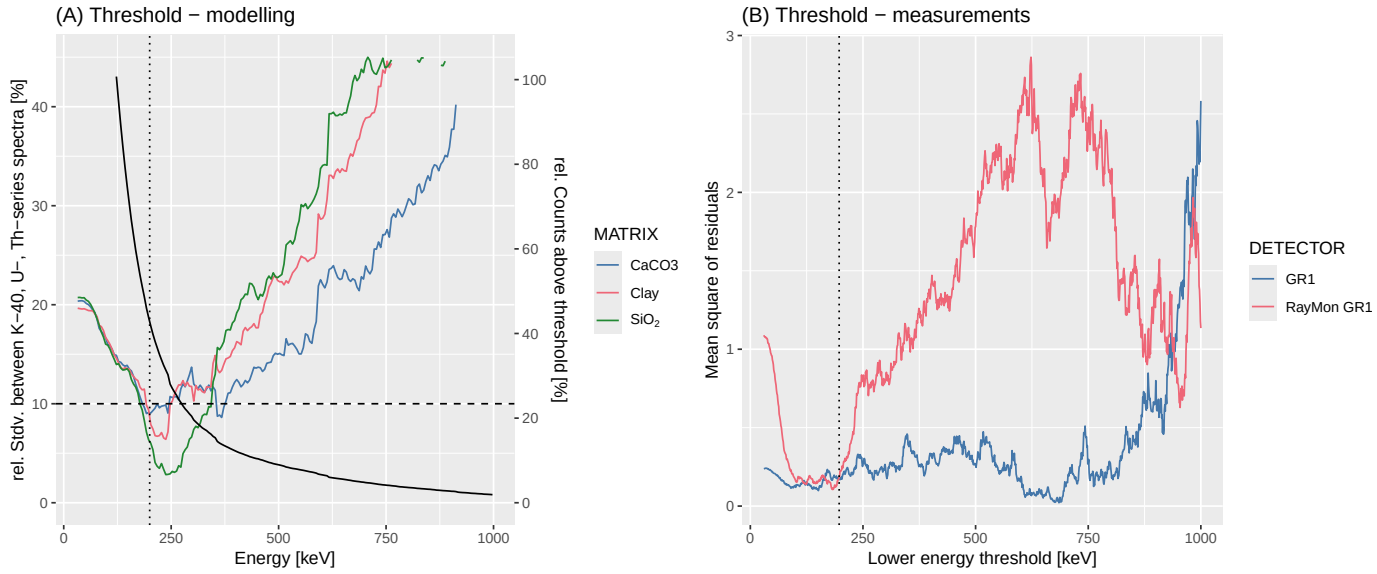

Figure 7. (A) GEANT4 modelling results, (B) mean square of residuals (MSWD) of the dose-rate model fitting against the chosen minimum energy threshold. Although both detectors differ due to the number of reference points, we conclude that the model fits best for a threshold (η) at ca 197 keV (dotted lines).

3.6 Dose-rate calibration

With now the threshold η defined, we can obtain our dose-rate model again with the function `gamma::dose_fit()`, but this time for a fixed energy threshold at 197 keV. The results are shown in Fig. 8 for the detector GR1 (Fig. 8A) and RayMon GR1 (Fig. 8B). Visual inspection confirms that the model fits the data excellently. However, the calibration curves differ slightly between the two detectors, which, given the similar slope, is likely due to the lower number of available data points. The fitting parameters of both regression lines overlap with uncertainties.

The package `'gamma'` automatically fits the data for the energy threshold *calculation* technique and the counting threshold *calculation* technique for a given η. In Fig. 8 we have shown only the latter. However, both values are accessible and saved in the file `CAL_heiLUM_V0.rda` we made accessible at Zenodo (Kreutzer et al., 2024). As a reminder, we converted the radionuclide concentrations from the reference sites to dose rates using conversion factors compiled by Cresswell et al. (2018). These values influence the slope and intercept of the calibration curves. Because it may be desirable to apply additional calibrations based on other available conversion factors we repeated the calibration using conversion factors from Adamiec and Aitken (1998), Guérin et al. (2011), and Liritzis et al. (2013) (see data on Zenodo: (Kreutzer et al., 2024).

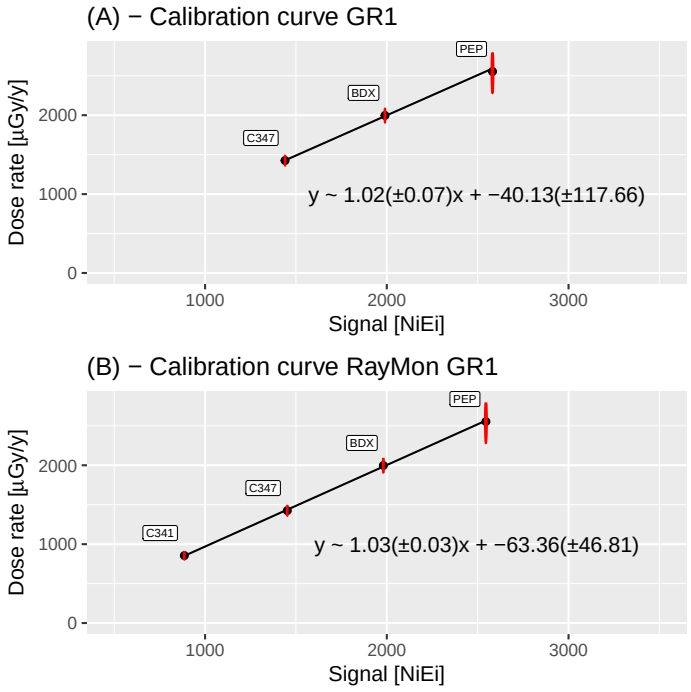

Figure 8. Dose-rate calibration curves for detector GR1 (A) and RayMon GR1 (B). Shown is the known γ-dose rate from the reference sites against the integrated energy signal between the threshold η (in keV) and $2800\,\mathrm{keV}$.

Table 2. Dry γ-dose rate results for the sample WH2024 obtained with different methods.

DETECTOR	U	σ_U	Th	σ_{Th}	K	σ_K	$\dot{D}_{\gamma-Ni}$	$\sigma_{\dot{D}_{\gamma-Ni}}$	$\dot{D}_{\gamma-NiEi}$	$\sigma_{\dot{D}_{\gamma-NiEi}}$	$\dot{D}_{\gamma-final}$	$\sigma_{\dot{D}_{\gamma-final}}$
GR1	NA	NA	NA	NA	NA	NA	1161.2	182.4	1080.9	147.6	1147.9	239.0
RayMon GR1	NA	NA	NA	NA	NA	NA	1086.5	90.2	1049.5	71.0	1093.5	117.1
µDose+ (05)	2.6	0.4	10.9	0.9	1.2	0.0	NA	NA	NA	NA	1115.7	37.0
µDose (25)	3.1	0.4	9.7	0.8	1.2	0.1	NA	NA	NA	NA	1132.5	34.9

Note:

U, Th concentrations in $\mu g\,g^{-1}$, K in % | dose rates in $\mu Gy\,a^{-1}$.

3.7 Cross-check against natural site

The measurements at the Weiße Hohl confirm once more that the two detectors exhibit very similar characteristics in terms of count rate efficiency (Fig. 9). Differences seem stochastic without visible systematic diversion over the measurement duration of $20\,\mathrm{min}$.

The water content from the sample site (sample code: WH2024) was estimated at 2.1 % and this value was used to correct $\dot{D}_\gamma$. Table 2 summarises the derived dose rate results for the two threshold integration techniques. $\dot{D}_{\gamma-final}$ is the arithmetic

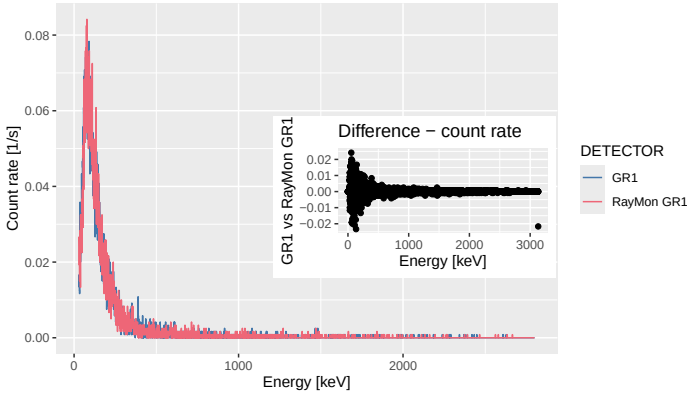

Figure 9. Gamma spectra recorded at Weiße Hohl (Germany) with the two detectors. The inset shows that the absolute count rate difference between the two detectors is randomly distributed.

average of the value of these two techniques. The results for GR1 and RayMon GR1 agree within 2σ uncertainties, whereas the average of GR1 appears to be slightly higher, and the uncertainty is almost twice as large. This observation is likely caused by the calibration of GR1 sitting on fewer data points. The comparison of $\dot{D}_\gamma$ against values derived from the radionuclide concentrations on WH2024 demonstrate a good agreement given the uncertainties associated with the field measurements. If we compare the CZT results (GR1 and RayMon GR1) with the laboratory derived $\dot{D}_\gamma$, both summarised as central values (e.g., Galbraith and Roberts, 2012) we obtained 1104.7 ± 105.2 µGy a^{-1} (CZT) and 1123.6 ± 24.7 µGy a^{-1} (laboratory).

The excellent agreement between in situ measurements and laboratory analysis is not utterly surprising, because we had picked the site because of its presumed matrix homogeneity. However, the selection of η, the energy threshold, is not free of subjectivity because our findings showed a range of equally acceptable values. To get a better feeling for the sensitivity of $\dot{D}_\gamma$ as a function of η for our detectors, we can calculate $\dot{D}_\gamma$ of the WH2024 for different values η. For this experiment on the energy calibrated spectra, we have to repeat the dose-rate calibration curve fitting and then predict the new dose rate given the newly derived calibration for η_i (in keV) with $i := \{30, 40, 50, ..., 530\}$. The upper integration energy was set to $2800\,\mathrm{keV}$ analogue to the previous calculations.

We assume that the laboratory results are the benchmark value we want reproduce. Figure 10 offers insight in the evolution of $\dot{D}_\gamma$ for GR1 (blue) and RayMon GR1 (red). The solid line is central value reference for WH2024 from laboratory measurements, and the dashed lines show the 2σ uncertainties (calculation after the Central Dose Model; Galbraith and Roberts (2012)). Regardless of the calibration-caused discrepancy between the two detectors, both detectors seem to form a plateau between ca $150\,\mathrm{keV}$ and $200\,\mathrm{keV}$ and overlap before falling systematically below the laboratory-derived reference value. Although the uncertainties of all analyses still overlap, it appears that for our setting and tested environment, the output is relatively insensitive to the exact value picked for η, as long as it sits within a certain threshold range.

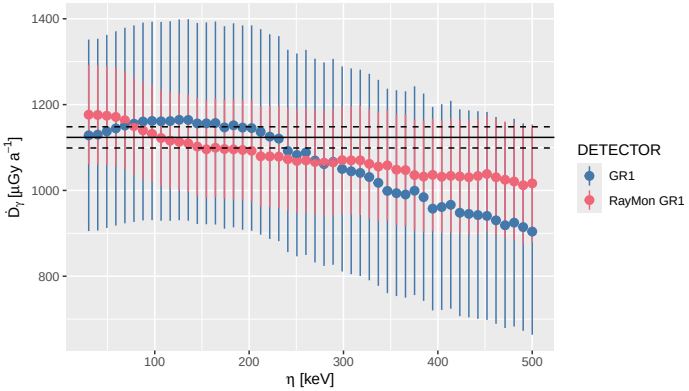

Figure 10. Estimations for $\dot{D}_\gamma$ for different values of η for the two investigated detectors. The solid line shows the $\dot{D}_\gamma$ of the measured site Weiße Hohl derived from laboratory radionuclide estimations and the dashed lines its uncertainties. For further details see maintext.

4 Discussion

Our study reported the performance and dose-rate calibration procedure of two portable semiconductor-based portable γ-ray spectrometers. Both devices host a similar CZT detector that can be operated at ambient temperature, i.e., in situations typical for environmental dose rate measurements as part of trapped-charge dating studies. Unlike literature reporting on γ-ray measurements in the field that used NaI or $LaBr_3$ probes with inch-size diameters, our detectors are considerably smaller (crystal volume $1\,\mathrm{cm}^3$), and the systems have a low power consumption, boosting their appeal for trapped-charge dating studies despite that no previous experience was available addressing our field of application. This seems surprising, given the body of available literature about CZT detectors. However, usually, those studies aim at nuclear radiation monitoring (e.g., Alam et al., 2021) or identifying artificial radio-nuclides in environmental studies (e.g., Rahman et al., 2013) for which such detectors are primarily designed.

On the plus side, this feature of the detectors simplified the energy/channel calibration with artificial radionuclides because of the detectors' sensitivity to those nuclides. Our energy calibration exhibited peak positions in excellent agreement for both detectors and we concluded that we could apply one single energy calibration. This approach was valid for us, but other detectors likely require seperate channel/energy calibration. Although we did not observe a shift in the channel/energy calibration with temperature during all experiments, we highly recommend an energy/channel calibration as part of the post-processing because all subsequent analyses depend on it.

Dating studies require an accurate reading of a sediment matrix's natural γ-radiation field of unknown radionuclide composition in a 4π geometry at the sampling position. Our study proved that both detectors can achieve this in a reasonable time of $20\,\mathrm{min}$. This value likely works for many environments typically encountered in trapped-charge dating applications. Still, it might be too short for accurate dose rate estimations in settings with a low amount of natural radionuclides or if higher precision is desired. Hence, in case of doubt, measurement times should be adjusted. We recommend a minimum measurement duration of $60\,\mathrm{min}$ to obtain the dose-rate calibration curve with a good counting statistics.

A crucial part of our contribution was the determination of the energy threshold η above which the dose rate results are independent of the photon origin. Given the highly comparable performance characteristics of the both detectors, our results can be easily used by others with the same detector without repeating all experiments. We applied two different methods (simulation, dose-rate response curve fitting) to determine this threshold and obtained comparable results around $200\,\mathrm{keV}$. This threshold is considerably lower than results obtained in studies with NaI or $LaBr_3$ probes that place η at ca $300\,\mathrm{keV}$ or higher (Mercier and Falguères, 2007; Guérin and Mercier, 2011; Duval and Arnold, 2013). This balances to some extent the lower absolute efficiency of the tiny CZT detectors because it allows exploiting a larger portion of the recorded spectrum. However, it should be noted that both approaches, simulation and dose-rate curve fitting, have different meanings. Under the assumption of correct input parameters, the simulation investigates the interaction of the γ-photons with matter for different scenarios and can hence truly determine a range above which the threshold assumption is valid. In other words, the simulation results have merit and provide a solid basis for setting the threshold. On the contrary, the dose-rate response curve fitting depends on the matrix composition of the host rock, which in our case, is very similar if translated into relative γ-dose rate contributions from the different radionuclides. We observed a matching pattern for the threshold from the measurements and the simulation, however, without the simulation our findings would be poorly supported. Means, the experimental data provide a good confirmation of the simulation results, but not vice versa. Without simulation, a meaningful determination requires measurements of emitters with pure radionuclide composition, such as the Oxford blocks (Rhodes and Schwenninger, 2007). The threshold quantified in our study, is likely not much different for detectors of similar size and with a comparable CZT detector. Therefore we argue that the threshold setting can be adapted if a simulation or a measurement is not possible. This suggestion is further supported by our tests of the Weiße Hohl measurement with shifting thresholds. The obtained γ-dose rate rate forms a plateau between $150\,\mathrm{keV}$ to $200\,\mathrm{keV}$ and minor difference in the detection characteristics will not bias the outcome for the γ-dose rate. Future work should investigate the calibration curve at very low and high dose rates and in very different environmental settings.

The $\dot{D}_\gamma$ results of the Weiße Hohl reflect mainly statistical variations of the different analytical methods. Striking but not puzzling are the relatively large uncertainties of the portable CZT detector results compared to the laboratory measurements and the larger uncertainties of GR1 compared to RayMon GR1, which seem to diminish the overall good performance. For GR1, the weaker performance (larger uncertainties) results from only having three calibration points available, which would disappear with an additional point. More generally, we argue that this outcome can be improved with more calibration points for the dose-rate calibration curve. Those points can be added at any time later, for instance, by measuring more sites around Clermont-Ferrand (Miallier et al., 2009).

Finally, what we did not expect of these CZT detectors but should be mention for completness is that our findings show that those detectors are unsuited for applying the "window" method in environments and for measurements durations typical for our field of application. For the determination of radionclide composition laboratory based analytical techniques are unmatched in their effectiviness and precision and they also allow to derive α and β-dose rate components.

5 Conclusions

The primary aim of our study was to test and evaluate the performance of two portable CZT detectors for deployment as active in situ detectors in trapped-charge dating applications. To that end, we measured spectra on natural reference sites with known radionuclide composition in France to derive a dose-rate calibration curves for our two detectors. Background measurements in a low-radiation setting exhibited negligible count rates that can be ignored.

To determine the optimal energy threshold above which the matrix composition of the measured site does not bias the integrated signal to γ-dose rate relation, we performed energy-matter interaction simulations using GEANT4. The simulation indicated a suitable energy threshold between 192.5 keV and 242.5 keV. We compared those results with signal-dose rate regression lines for two different integration techniques (count threshold, energy threshold technique) and we found a value of 217 keV for the counting threshold integration and 182 keV for energy counting integration technique. We settled on the arithmetic average of both results at 197 keV. To record a γ-dose rate in typical natural sediment environments, we recommend a measurement time of at least $20\,\mathrm{min}$.

A check of our results through measurements at the homogeneous loess deposit near Heidelberg for which we derived the radionuclide composition in the laboratory, confirmed an excellent match of field and laboratory methods, however, with considerably larger (but perhaps more realistic) uncertainties for results from the CZT detectors. Finally, we argued that refined calibrations can further reduce those uncertainties on more sites. Future work may want to extend our calibration curves and explore the performance of the detector in more extreme (low and high) natural radiation fields.

. Raw and partly processed data and R code used in this study is available on Zenodo (https://doi.org/10.5281/zenodo.13731839; last access: 2024-09-10).

. SK: Writing – original draft, Validation, Methodology, Formal analysis, Conceptualization, Funding acquisition, Data curation, Software. LM: Writing – review and editing, Methodology, Formal analysis. DM: Writing – review and editing, Resources. NM: Writing – review and editing, Methodology, Formal analysis, Conceptualization.

. We declare no conflict of interest and did not receive funds other than what was stated. The Heidelberg Luminescence Laboratory procured the tested systems with its own funds, and we did not liaise with the supplier of the measurement systems for this study.

. Our contribution aims to provide information on the practical use of systems available commercially off-shelf to the trapped-charge dating community and report calibration and performance results. However, we do not favour a particular supplier, and our manuscript must not be understood as a purchase recommendation.

. We thank Nicolas Frerebeau for his very responsive support as maintainer of the
R package ‘gamma’. We thank Maryam Heydari for performing the measurements at the Weiße Hohl.

References

Adamiec, G. and Aitken, M. J.: Dose-rate conversion factors: update, Ancient TL, 16, 37–50, http://ancienttl.org/ATL_16-2_1998/ATL_16-2_Adamiec_p37-50.pdf (last access: 2024-09-02), 1998.

Agostinelli, S., Allison, J., Amako, K., Apostolakis, J., Araujo, H., Arce, P., Asai, M., Axen, D., Banerjee, S., Barrand, G., Behner, F., Bellagamba, L., Boudreau, J., Broglia, L., Brunengo, A., Burkhardt, H., Chauvie, S., Chuma, J., Chytracek, R., Cooperman, G., Cosmo, G., Degtyarenko, P., Dell'Acqua, A., Depaola, G., Dietrich, D., Enami, R., Feliciello, A., Ferguson, C., Fesefeldt, H., Folger, G., Foppiano, F., Forti, A., Garelli, S., Giani, S., Giannitrapani, R., Gibin, D., Cadenas, J. J. G., González, I., Abril, G. G., Greeniaus, G., Greiner, W., Grichine, V., Grossheim, A., Guatelli, S., Gumplinger, P., Hamatsu, R., Hashimoto, K., Hasui, H., Heikkinen, A., Howard, A., Ivanchenko, V., Johnson, A., Jones, F. W., Kallenbach, J., Kanaya, N., Kawabata, M., Kawabata, Y., Kawaguti, M., Kelner, S., Kent, P., Kimura, A., Kodama, T., Kokoulin, R., Kossov, M., Kurashige, H., Lamanna, E., Lampén, T., Lara, V., Lefebure, V., Lei, F., Liendl, M., Lockman, W., Longo, F., Magni, S., Maire, M., Medernach, E., Minamimoto, K., de Freitas, P. M., Morita, Y., Murakami, K., Nagamatu, M., Nartallo, R., Nieminen, P., Nishimura, T., Ohtsubo, K., Okamura, M., O'Neale, S., Oohata, Y., Paech, K., Perl, J., Pfeiffer, A., Pia, M. G., Ranjard, F., Rybin, A., Sadilov, S., Salvo, E. D., Santin, G., Sasaki, T., Savvas, N., Sawada, Y., Scherer, S., Sei, S., Sirotenko, V., Smith, D., Starkov, N., Stoecker, H., Sulkimo, J., Takahata, M., Tanaka, S., Tcherniaev, E., Tehrani, E. S., Tropeano, M., Truscott, P., Uno, H., Urban, L., Urban, P., Verderi, M., Walkden, A., Wander, W., Weber, H., Wellisch, J. P., Wenaus, T., Williams, D. C., Wright, D., Yamada, T., Yoshida, H., and Zschiesche, D.: GEANT4—a simulation toolkit, Nuclear Instruments and Methods in Physics Research Section A: Accelerators, Spectrometers, Detectors and Associated Equipment, 506, 250–303, https://doi.org/10.1016/s0168-9002(03)01368-8, 2003.

Aitken, M. J.: Thermoluminescence dating, Studies in archaeological science., Academic Press, London, ISBN 978-0-12-046381-7, 1985.

Alam, M. D., Nasim, S. S., and Hasan, S.: Recent progress in CdZnTe based room temperature detectors for nuclear radiation monitoring, Progress in Nuclear Energy, 140, 103 918, https://doi.org/10.1016/j.pnucene.2021.103918, 2021.

Alexiev, D., Mo, L., Prokopovich, D. A., Smith, M. L., and Matuchova, M.: Comparison of LaBr3:Ce and LaCl3:Ce With NaI(Tl) and Cadmium Zinc Telluride (CZT) Detectors, IEEE Transactions on Nuclear Science, 55, 1174–1177, https://doi.org/10.1109/TNS.2008.922837, 2008.

Antoine, P., Rousseau, D.-D., Zöller, L., Lang, A., Munaut, A.-V., Hatté, C., and Fontugne, M.: High-resolution record of the last Interglacial-glacial cycle in the Nussloch loess-palaeosol sequences, Upper Rhine Area, Germany, Quaternary International, 76/77, 211–229, 2001.

Arnold, L. J., Duval, M., Falguères, C., Bahain, J. J., and Demuro, M.: Portable gamma spectrometry with cerium-doped lanthanum bromide scintillators: Suitability assessments for luminescence and electron spin resonance dating applications, Radiation Measurements, 47, 6–18, https://doi.org/10.1016/j.radmeas.2011.09.001, 2012.

Bosq, M., Kreutzer, S., Bertran, P., Lanos, P., Dufresne, P., and Schmidt, C.: Last Glacial loess in Europe: luminescence database and chronology of deposition, Earth System Science Data, https://doi.org/10.5194/essd-2023-105, 2023.

Bu, M., Murray, A. S., Kook, M., Buylaert, J.-P., and Thomsen, K. J.: The Application of Full Spectrum Analysis to NaI(Tl) Gamma Spectrometry for the Determination of Burial Dose Rates, Geochronometria, 48, 161–170, https://doi.org/10.2478/geochr-2020-0009, 2021.

Cresswell, A. J., Carter, J., and Sanderson, D. C. W.: Dose rate conversion parameters: Assessment of nuclear data, Radiation Measurements, 120, 195–201, https://doi.org/10.1016/j.radmeas.2018.02.007, 2018.

Duval, M. and Arnold, L.: Field gamma dose-rate assessment in natural sedimentary contexts using LaBr3(Ce) and NaI(Tl) probes: A comparison between the “threshold” and “windows” techniques, Applied Radiation and Isotopes, 74, 36–45, https://doi.org/10.1016/j.apradiso.2012.12.006, 2013.

Frerebeau, N.: khroma: Colour Schemes for Scientific Data Visualization, Université Bordeaux Montaigne, Pessac, France, https://doi.org/10.5281/zenodo.1472077, R package version 1.14.0, 2024.

Frerebeau, N., Lebrun, B., Paradol, G., and Kreutzer, S.: gamma: Dose Rate Estimation from in-Situ Gamma-Ray Spectrometry, Université Bordeaux Montaigne, Pessac, France, https://doi.org/10.32614/CRAN.package.gamma, r package version 1.0.5.9000, 2024.

Galbraith, R. F. and Roberts, R. G.: Statistical aspects of equivalent dose and error calculation and display in OSL dating: An overview and some recommendations, Quaternary Geochronology, 11, 1–27, https://doi.org/10.1016/j.quageo.2012.04.020, 2012.

Gilmore, G. R.: Practical gamma-ray spectrometry, John wiley \& sons, ltd, John Wiley \& Sons, Ltd, 2nd edition edn., 2008.

Godfrey-Smith, D. I., Scallion, P., and Clarke, M. L.: BETA DOSIMETRY OF POTASSIUM FELDSPARS IN SEDIMENT EXTRACTS USING IMAGING MICROPROBE ANALYSIS AND BETA COUNTING, Geochronometria, 24, 7–12, http://www.geochronometria.pl/pdf/geo_24/Geo24_2.pdf (last access: 2024-09-02), 2005.

Guérin, G. and Mercier, N.: Determining gamma dose rates by field gamma spectroscopy in sedimentary media: Results of Monte Carlo simulations, Radiation Measurements, 46, 190–195, https://doi.org/10.1016/j.radmeas.2010.10.003, 2011.

Guérin, G., Mercier, N., and Adamiec, G.: Dose-rate conversion factors: update, Ancient TL, 29, 5–8, http://ancienttl.org/ATL_29-1_2011/ATL_29-1_Guerin_p5-8.pdf (last access: 2024-09-02), 2011.

Guérin, G., Mercier, N., Nathan, R., Adamiec, G., and Lefrais, Y.: On the use of the infinite matrix assumption and associated concepts: A critical review, Radiation Measurements, 47, 778–785, https://doi.org/10.1016/j.radmeas.2012.04.004, 2012.

Hutton, J. T. and Prescott, J. R.: Field and laboratory measurements of low-level thorium, uranium and potassium, International Journal of Radiation Applications and Instrumentation. Part D. Nuclear Tracks and Radiation Measurements, 20, 367–370, https://doi.org/10.1016/1359-0189(92)90066-5, 1992.

Kalchgruber, R. and Wagner, G. A.: Separate assessment of natural beta and gamma dose-rates with TL from single-crystal chips, Radiation Measurements, 41, 154–162, https://doi.org/10.1016/j.radmeas.2005.04.002, 2006.

Kalchgruber, R., Fuchs, M., Murray, A. S., and Wagner, G. A.: Evaluating dose-rate distributions in natural sediments using α-Al2O3:C grains, Radiation Measurements, 37, 293–297, https://doi.org/10.1016/S1350-4487(03)00012-X, 2003.

Kolb, T., Tudyka, K., Kadereit, A., Lomax, J., Poręba, G., Zander, A., Zipf, L., and Fuchs, M.: The μDose system: determination of environmental dose rates by combined alpha and beta counting – performance tests and practical experiences, Geochronology, 4, 1–31, https://doi.org/10.5194/gchron-4-1-2022, 2022.

Kreutzer, S., Martin, L., Guérin, G., Tribolo, C., Selva, P., and Mercier, N.: Environmental dose rate determination using a passive dosimeter: Techniques and workflow for alpha-Al_2O_3:C chips, Geochronometria, 45, 56–67, https://doi.org/10.1515/geochr-2015-0086, 2018.

Kreutzer, S., Martin, L., Miallier, D., and Mercier, N.: Dataset: Environmental Gamma Dose Rate Measurements using CZT Detectors, https://doi.org/10.5281/zenodo.13731839, 2024.

Lebrun, B., Frerebeau, N., Paradol, G., Guérin, G., Mercier, N., Tribolo, C., Lahaye, C., and Magali, R.: gamma: An R package for dose rate estimation from in-situ gamma-ray spectrometry measurements, Ancient TL, 38, 11–15, http://ancienttl.org/ATL_38-2_2020/ATL_38-2_Lebrun_p1-5.pdf (last access: 2024-09-02), 2020.

Limousin, O.: New trends in CdTe and CdZnTe detectors for X- and gamma-ray applications, Nuclear Instruments and Methods in Physics Research Section A: Accelerators, Spectrometers, Detectors and Associated Equipment, 504, 24–37, https://doi.org/10.1016/S0168-9002(03)00745-9, 2003.

Liritzis, I., Stamoulis, K., Papachristodoulou, C., and Ioannides, K.: A re-evaluation of radiation dose-rate conversion factors, Mediterranean Archaeology and Archaeometry, 12, 1–15, http://maajournal.com/Issues/2012/pdf/FullTextLiritzis.pdf (last access: 2024-09-02), 2013.

Løvborg, L. and Kirkegaard, P.: Response of $3'' \times 3''$ NaI(Tl) detectors to terrestrial gamma radiation, Nuclear Instruments and Methods, 121, 239–251, https://doi.org/10.1016/0029-554x(74)90072-x, 1974.

Martin, L., Duval, M., and Arnold, L. J.: To what extent do field conditions affect gamma dose rate determination using portable gamma spectrometry?, Radiation Physics and Chemistry, 216, 111 365, https://doi.org/10.1016/j.radphyschem.2023.111365, 2024.

Mauz, B., Hubmer, A., Bahl, C., Lettner, H., and Lang, A.: Comparing two efficiency calibration methods used in gamma spectrometry, Ancient TL, 39, 12–17, http://ancienttl.org/ATL_39-2_2021/ATL_39-2_Mauz_p12-17.pdf (last access: 2024-09-02), 2021.

Mercier, N. and Falguères, C.: Field gamma dose-rate measurement with a NaI(Tl) detector: re-evaluation of the technique, Ancient TL, 25, 1–4, http://ancienttl.org/ATL_25-1_2007/ATL_25-1_Mercier_p1-4.pdf (last access: 2024-09-02), 2007.

Miallier, D., Guérin, G., Mercier, N., Pilleyre, T., and Sanzelle, S.: The Clermont radiometric reference rocks: a convenient tool for dosimetric purposes, Ancient TL, 27, 37–44, http://ancienttl.org/ATL_27-2_2009/ATL_27-2_Miallier_p37-44.pdf (last access: 2024-09-02), 2009.

Preusser, F. and Kasper, H. U.: Comparison of dose rate determination using high-resolution gamma spectrometry and inductively coupled plasma - mass spectrometry, Ancient TL, 19, 19–23, http://ancienttl.org/ATL_19-1_2001/ATL_19-1_Preusser_p19-23.pdf (last access: 2024-09-02), 2001.

R Core Team: R: A language and environment for statistical computing, https://r-project.org/ (last access: 2024-09-02), 2024.

Rahman, R., Plater, A. J., Nolan, P. J., and Appleby, P. G.: Assessing CZT detector performance for environmental radioactivity investigations, Radiation Protection Dosimetry, 154, 477–482, https://doi.org/10.1093/rpd/ncs253, 2013.

Rhodes, E. J. and Schwenninger, J. L.: Dose rates and radioisotope concentrations in the concrete calibration blocks at Oxford, Ancient TL, 25, 5–8, http://ancienttl.org/ATL_25-1_2007/ATL_25-1_Rhodes_p5-8.pdf (last access: 2024-09-02), 2007.

Richter, D., Dombrowski, H., Neumaier, S., Guibert, P., and Zink, A. C.: Environmental gamma dosimetry with OSL of -Al2O3:C for in situ sediment measurements, Radiation Protection Dosimetry, 141, 27–35, https://doi.org/10.1093/rpd/ncq146, 2010.

Rieser, U.: Low-level gamma-spektrometrie zum zwecke der dosisleistungsbestimmung bei der lumineszenz datierung, Diplomarbeit (unpublished), Ruprecht-Karls University of Heidelberg, Heidelberg, 1991.

Sanderson, D. C. W. and Murphy, S.: Using simple portable OSL measurements and laboratory characterisation to help understand complex and heterogeneous sediment sequences for luminescence dating, Quaternary Geochronology, 5, 299–305, https://doi.org/10.1016/j.quageo.2009.02.001, 2010.

Scheiber, C. and Chambron, J.: CdTe detectors in medicine: a review of current applications and future perspectives, Nuclear Instruments and Methods in Physics Research Section A: Accelerators, Spectrometers, Detectors and Associated Equipment, 322, 604–614, https://doi.org/10.1016/0168-9002(92)91239-6, 1992.

Tudyka, K., Miłosz, S., Adamiec, G., Bluszcz, A., Poręba, G., Paszkowski, Ł., and Kolarczyk, A.: μDose_ A compact system for environmental radioactivity and dose rate measurement, Radiation Measurements, 118, 8–13, https://doi.org/10.1016/j.radmeas.2018.07.016, 2018.

Tudyka, K., Kłosok, K., Gosek, M., Kolarczyk, A., Miłosz, S., Szymak, A., Pilśniak, A., Moska, P., and Poręba, G.: μDOSE+: Environmental radioactivity and dose rate measurement system with active shielding boosted by machine learning, Measurement, 234, 114 854, https://doi.org/10.1016/j.measurement.2024.114854, 2024.

Verger, L., Bonnefoy, J. P., Glasser, F., and Ouvrier-Buffet, P.: New Developments in CdTe and CdZnTe Detectors for X and y-Ray Applications, Journal of Electronic Materials, 26, 738–744, https://doi.org/10.1007/s11664-997-0225-2, 1997.

Wickham, H.: ggplot2: Elegant Graphics for Data Analysis, Springer-Verlag New York, ISBN 978-3-319-24277-4, https://ggplot2.tidyverse.org (last access: 2024-09-02), 2016.

Zöller, L. and Pernicka, E.: A note on overcounting in alpha-counters and its elimination, Ancient TL, 7, 11–14, http://ancienttl.org/ATL_07-1_1989/ATL_07-1_Zoller_p11-14.pdf (last access: 2024-09-02), 1989.